Chaotic Modeling and Simulation (CMSIM) 4: 479–491, 2017

Quantum correspondence of classical phase space structures in the correlation diagram of eigenenergies versus Planck constant

H. Párraga[1], F. J. Arranz[1], R. M. Benito[1], and F. Borondo[2]

[1] Grupo de Sistemas Complejos, Universidad Politécnica de Madrid, 28040 Madrid, Spain
(E-mail: fj.arranz@upm.es, rosamaria.benito@upm.es)

[2] Departamento de Química and Instituto de Ciencias Matemáticas (ICMAT), Universidad Autónoma de Madrid, 28049 Madrid, Spain
(E-mail: f.borondo@uam.es)

Abstract. The correlation diagram of eigenenergies versus Planck constant has been proven as a suitable and useful tool for the study of the quantum manifestations of chaos in molecular systems. In this paper, we study the dynamics of the nonlinear LiCN and highly nonlinear KCN molecular systems, showing how the regular classical structures (Kolmogorov-Arnold-Moser tori) embedded in the chaotic sea in phase space (mixed-chaos regime) are manifested in the correlation diagram as emerging diabatic states, which can remain hidden if only a fixed value of the Planck constant is considered (typically $\hbar = 1$ a.u.). Additionally, the quantum transition from order to chaos is studied, in the framework of the scars frontier reported in the literature, for the two-regions (regular and chaotic) LiCN correlation diagram and for the apparently chaotic (mixed-chaos) KCN correlation diagram, leading to the proposal of a schematic correlation diagram arrangement for a generic molecular system.
Keywords: Quantum chaos, Quantum-classical correspondence, Eigenenergies correlation diagram, Nonlinear molecular systems.

1 Introduction

The correspondence between classical mechanics and quantum mechanics remains a topic of interest, as evidenced by the abundant recent literature about it. Since the correspondence for integrable systems was explained essentially in terms of the EBK (Einstein-Brillouin-Keller) quantization [1], and the correspondence for chaotic (ergodic) systems in terms of the Gutzwiller trace formula [2], the focus is on systems with the so-called mixed-chaos behavior, where regular and chaotic structures coexist.

Moreover, one of the most solid theoretical tools to study the quantum-classical correspondence is random matrix theory [3] and, especially, the level statistics derived from it, where the statistical behavior of the neighboring

Received: 6 June 2017 / Accepted: 25 October 2017

ISSN 2241-0503

eigenenergy levels as the strength of the perturbation changes is analyzed. Notice that the eigenenergies spectrum versus the strength of the perturbation constitutes the corresponding correlation diagram, being the correlation diagram versus Planck constant a proven useful tool for the study of the quantum manifestations of chaos [4]. Additionally, in contrast with toy systems (as is the case, for example, of quantum maps), we think that realistic systems (as is the case of molecular systems) are especially interesting.

In this paper, we present a study on the correspondence between classical structures in phase space and quantum structures in the correlation diagram versus Planck constant, for molecular systems with mixed-chaos behavior, showing specific results for LiCN and KCN molecules.

2 Molecular model and calculations

2.1 Hamiltonian molecular model

Both systems studied in this work correspond to triatomic cyanide molecules XCN (with $X = \mathrm{Li}, \mathrm{K}$), where the length between C and N atoms can be fixed at its equilibrium value, since the CN bond is much stronger than the interactions with atom X, so that an adiabatic decoupling of the involved degree of freedom is suitable. Namely, we study the motion of atom X around the dimer CN. The corresponding Hamiltonian function for the purely vibrational dynamics (i.e., without rotation) is given in Jacobi coordinates by

$$H = \frac{P_R^2}{2\mu_1} + \frac{P_\theta^2}{2}\left(\frac{1}{\mu_1 R^2} + \frac{1}{\mu_2 r_{\mathrm{eq}}^2}\right) + V(R,\theta), \tag{1}$$

where $\mu_1 = m_X(m_\mathrm{C}+m_\mathrm{N})/(m_X+m_\mathrm{C}+m_\mathrm{N})$ and $\mu_2 = m_\mathrm{C}m_\mathrm{N}/(m_\mathrm{C}+m_\mathrm{N})$ are reduced masses (being m_X, m_C, and m_N the corresponding atomic masses), r_{eq} is the fixed C-N equilibrium length ($r_{\mathrm{eq}} = 2.19$ a.u. for $X = \mathrm{Li}$ and $r_{\mathrm{eq}} = 2.22$ a.u. for $X = \mathrm{K}$), R is the distance between the CN dimer center of mass and the X atom, and θ is the angle formed by the corresponding R and r_{eq} directions, with $\theta = 0$ and $\theta = \pi$ rad for the linear configurations X-CN and CN-X, respectively. Clearly, P_R and P_θ are the corresponding conjugate momenta, and $V(R,\theta)$ is the potential energy function describing the vibrational interactions in each molecular system.

For the potential energy function, an analytic fit to *ab initio* quantum calculations has been taken in each case from the literature [5,6]. The potential energy function $V(R,\theta)$, along with the minimum energy path $R_{\mathrm{eq}}(\theta)$ connecting minima and saddles, and the energy profile $V_{\mathrm{eq}}(\theta) = V\big(R_{\mathrm{eq}}(\theta),\theta\big)$ along the minimum energy path, are depicted in Fig. 1 for both molecular systems. Observe that the behavior of potential energy along the angular coordinate θ is very anharmonic in both cases. Moreover, in the LiCN molecular system both linear configurations, $\theta = 0$ and $\theta = \pi$ rad, have stable equilibrium points, being the most stable one at $\theta = \pi$ rad. However, in the KCN molecular system only linear configuration at $\theta = 0$ has a stable, albeit shallow, equilibrium point, the other linear configuration at $\theta = \pi$ rad corresponding to a saddle point. Notice that, in KCN case the most stable configuration is a triangular configuration.

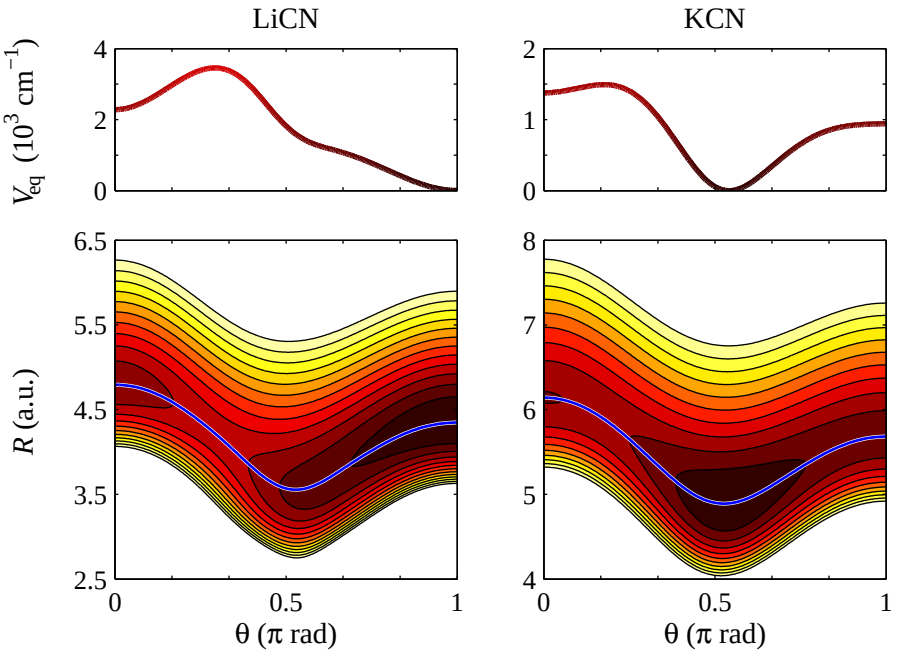

Fig. 1. Potential energy function for LiCN (left panels) and KCN (right panels) molecular systems. (Bottom) Contour plot representation spaced 1000 cm^{-1} for LiCN and 700 cm^{-1} for KCN. The minimum energy path connecting minima and saddles in each energy surface has been superimposed in blue thick line. (Top) Potential energy profile along the minimum energy path.

2.2 Classical calculations

The Hamilton equations of motion corresponding to Eq. (1) have been built and standard numerical integration used to obtain trajectories for each molecular system. In order to get a suitable graphical representation of the phase space structure, we have calculated composite Poincaré surfaces of section along the minimum energy path for increasing energies. For this purpose, analytic expressions $R_{\rm eq}(\theta)$ for each minimum energy path fitted to a Fourier series, adequate for differential transformations, have been used.

In this way, the canonical transformation

$$\rho = R - R_{\rm eq}(\theta), \qquad \vartheta = \theta, \tag{2a}$$

$$P_\rho = P_R, \qquad P_\vartheta = P_\theta + P_R \frac{dR_{\rm eq}}{d\theta}, \tag{2b}$$

is made, so that, for a given energy E, a Poincaré surface of section along the minimum energy path is defined, in (ϑ, P_ϑ) coordinates, by making $\rho = 0$ and choosing an arbitrary branch (the negative one in our calculations) in the second order equation for P_ρ that arise from the Hamiltonian conservation $H(\rho, \vartheta, P_\rho, P_\vartheta) = E$. Finally, all calculated points from the Poincaré surface

of section are folded into the interval $\vartheta \in [0, \pi]$ rad, taking into account the symmetry of both molecular systems.

Moreover, the relevant periodic orbits have been obtained, taking advantage of the symmetry of both systems, by means of the propagation of symmetry lines [7].

2.3 Quantum calculations

In order to obtain the eigenfunctions and eigenenergies of the Hamiltonian operator corresponding to the Hamiltonian function in Eq. (1) for both molecular systems, the *discrete variable representation–distributed Gaussian basis* method of Bačić and Light [8] was used.

In this way, for the LiCN system, by using a final basis set of around 400 ray eigenvectors lying in 50 angular rays (for decreasing $\hbar$ from 1 a.u. to 0.04 a.u. the number of rays increases up to 180), around 130 low lying eigenfunctions $\langle R\,\theta\,|n\rangle_{\hbar}$ $(n = 1, \ldots, 130)$ with their eigenenergies converged to within 1 cm^{-1} were obtained at values $\hbar = \{0.04, 0.05, \ldots, 3.00\}$ a.u., leading to the corresponding correlation diagram of eigenenergies versus Planck constant.

Similarly, for the KCN system, by using a final basis set of around 1000 ray eigenvectors lying in 50 angular rays (the number of rays increasing up to 120 for decreasing $\hbar$ from 0.5 a.u. to 0.1 a.u.), around 300 low lying eigenfunctions $\langle R\,\theta\,|n\rangle_{\hbar}$ $(n = 1, \ldots, 300)$ with their eigenenergies converged to within 1 cm^{-1} were obtained at values $\hbar = \{0.10, 0.11, \ldots, 3.00\}$ a.u., leading to the corresponding correlation diagram.

Notice that, due to numerical accuracy issues, the correlation diagram for $\hbar < 0.04$ a.u. in LiCN case, and for $\hbar < 0.10$ a.u. in KCN case, could not be calculated correctly.

3 Results and discussion

3.1 Classical dynamics: Poincaré surface of section

In order to describe the behavior of the LiCN molecular system as energy increases, composite Poincaré surfaces of section at different energies are depicted in Fig. 2.

Observe that at $E = 1500$ cm^{-1} the dynamics is completely regular. Notice that main resonances ω_ϑ:ω_ρ arising from Poincaré-Birkhoff theorem [9] have been specifically represented, namely 1:6, 1:7, 1:8, 1:9, 1:10, and again 1:10. Moreover, at $E = 2300$ cm^{-1} the mechanism of Chirikov [9] has originated an extended chaotic region, albeit main tori around $(\vartheta, P_\vartheta) = (\pi, 0)$ (rad, a.u.) remain. Note the existence of the near to energy boundary chain of islands immersed in the chaotic sea, corresponding to a 1:8 resonance. Interleaved in this 1:8 stable resonance there exists a complementary 1:8 unstable resonance not visible on the composite Poincaré surface of section. Finally, at $E = 4000$ cm^{-1} chaos is extended in phase space, however, regular regions corresponding to both Li-CN and CN-Li linear configurations endure.

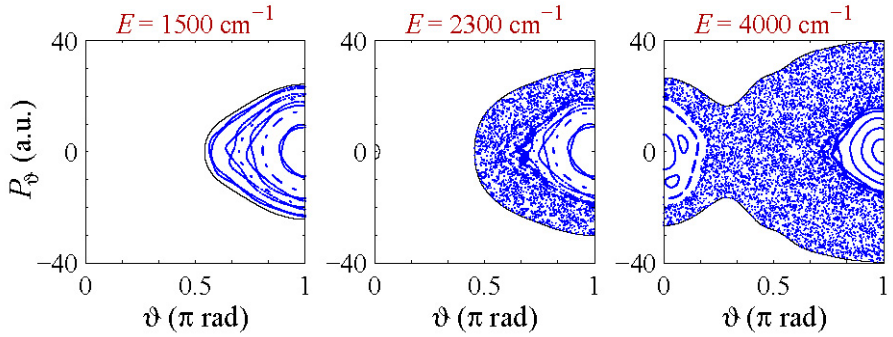

Fig. 2. Composite Poincaré surfaces of section along the minimum energy path for the LiCN molecular system at different energies, showing the transition from order to chaos and the mixed-chaos evolution as energy increases.

On the other hand, a representative selection of composite Poincaré surfaces of section at increasing energies for the KCN molecular system is depicted in Fig. 3.

The first row of panels ($E = 45, 65, 145$ cm^{-1}) illustrates the onset of chaos in this system. We can observe that, according to Poincaré-Birkhoff and Kolmogorov-Arnold-Moser theorems [9], the main periodic orbit corresponding to central tori at $E = 45$ cm^{-1} suffers a pitchfork bifurcation clearly visible at $E = 65$ cm^{-1}. Then, following the mechanism of Chirikov, the separatrix that arises from this bifurcation breaks, leading to an extended chaotic region at $E = 145$ cm^{-1}.

The second row of panels ($E = 250, 290, 320$ cm^{-1}) shows the evolution of the two main 1:2 stable resonances, corresponding to the chain of two islands already existing at $E = 45$ cm^{-1}, and the chain of two islands arising from the pitchfork bifurcation of the main periodic orbit depicted in the first row of panels. Observe that the former 1:2 resonance suffers a pitchfork bifurcation, apparent at $E = 250$ cm^{-1}, becoming unstable. The other stable 1:2 resonance remains stable at $E = 290$ cm^{-1}, whilst the separatrix that arose from the pitchfork bifurcation of the former 1:2 resonance has broken, leading to extended chaos in this region. Ultimately, the stable 1:2 resonance also suffers a pitchfork bifurcation, clearly visible at $E = 320$ cm^{-1}.

The third row of panels ($E = 1300, 1500, 2400$ cm^{-1}) is devoted to the emergence of stable structures at both linear molecular configurations, K-CN and CN-K. Observe that at $E = 1300$ cm^{-1} the linear saddle configuration, corresponding to $\vartheta = \pi$ rad, is widely attainable, and chaotic behavior is apparently widespread over the whole available phase space. However, when energy is increased, new stable structures emerge. Thus, at $E = 1500$ cm^{-1} the linear minimum configuration, corresponding to $\vartheta = 0$, is broadly reachable, and stable structures (namely, a main tori family at the minimum with an associated chain of four islands around it) appear in the linear minimum region. Observe that, surprisingly, at $E = 1500$ cm^{-1} a stable structure also appears in the linear saddle region. At $E = 2400$ cm^{-1} this stable structure has expanded,

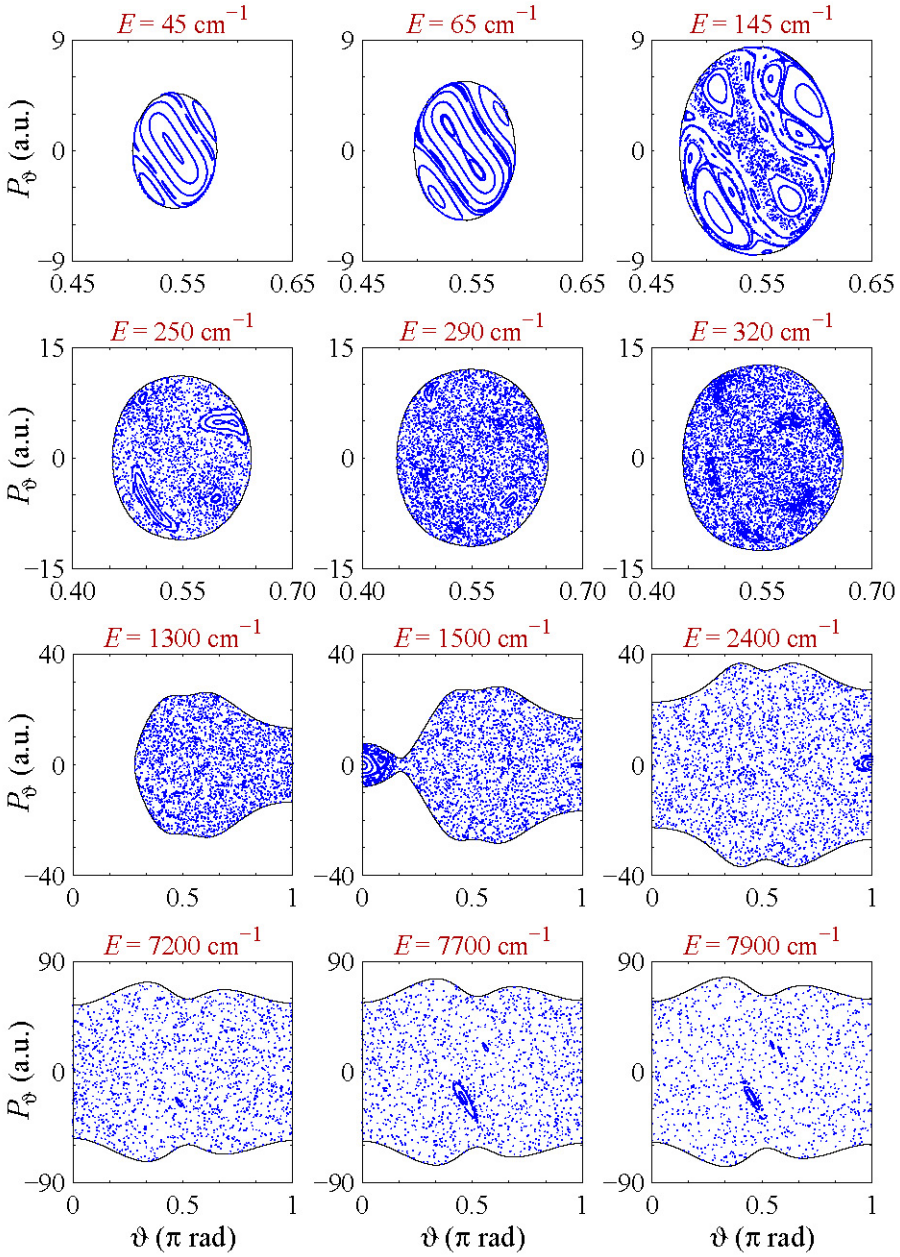

Fig. 3. Same as described in the caption of Fig. 2 for the KCN molecular system.

including a chain of six islands around it, whilst the stable structures in the linear minimum region has become chaotic.

Last, as is shown in the fourth row of panels ($E = 7200, 7700, 7900$ cm^{-1}), new stable structures emerge at very high energy. Thus, at $E = 7200$ cm^{-1} we

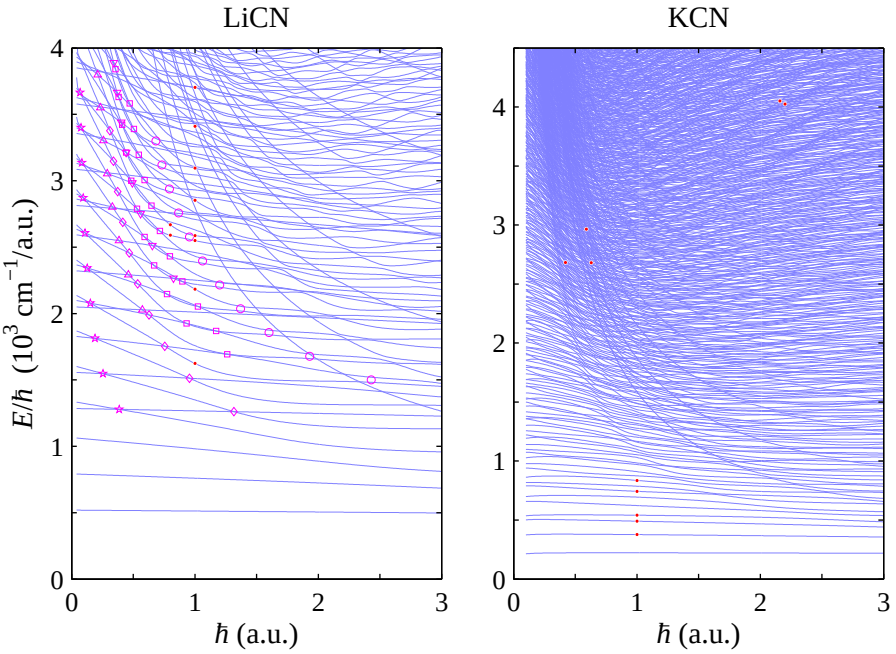

Fig. 4. Correlation diagram of eigenenergies versus Planck constant for LiCN (left panel) and KCN (right panel) molecular systems. On grounds of graphical clarity, energy is divided by Planck constant. The states corresponding to wavefunctions represented in Figs. 5 and 6 are marked with red dots. Additionally, main series of Fermi resonances in the regular region of the LiCN correlation diagram are marked with magenta open symbols (see Table 1).

can observe the appearance of a small tori family in the region around $\vartheta = \pi/2$ rad with $P_\vartheta < 0$. At $E = 7700$ cm^{-1} this tori family has extended, and a new tori family has emerged in the region around $\vartheta = \pi/2$ rad with $P_\vartheta > 0$. At $E = 7900$ cm^{-1} the former tori family with $P_\vartheta < 0$ still remains, and a second tori family has emerged with $P_\vartheta > 0$. All these regular structures correspond to *hinge* motion (angular back and forth motion) of the atom K around the group CN, where $P_\vartheta < 0$ corresponds to hinge motion around CN-K linear configuration and $P_\vartheta > 0$ corresponds to hinge motion around K-CN linear configuration.

3.2 Quantum eigenstates: Correlation diagram

The correlation diagram of eigenenergies versus Planck constant for the LiCN molecular system has been depicted in the left panel of Fig. 4. Note that, in order to make the picture more readable, energy has been divided by Planck constant. Representative states at the true value $\hbar = 1$ a.u. have been marked with red dots and the corresponding wavefunctions depicted in Fig. 5.

All states at $\hbar = 1$ a.u. from $n = 1$ to $n = 23$ correspond to regular states, that is, we can assign quantum numbers $n_\perp$ and $n_\parallel$ by counting nodal lines

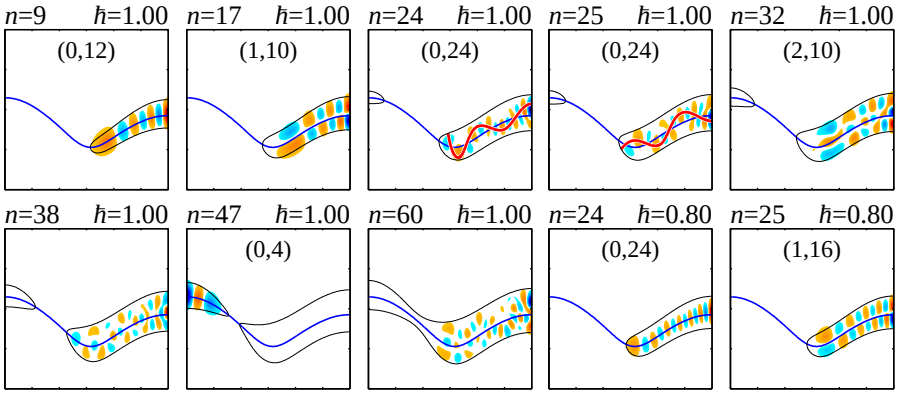

Fig. 5. Wavefunctions $\langle R\,\theta|n\rangle_\hbar$ of the LiCN eigenstates marked with red dots in Fig. 4 represented in color scale. The minimum energy path and the corresponding eigenenergy contour have also been represented as blue line and black line, respectively. Where appropriate, the involved periodic orbits have been superimposed as red thick lines, and quantum numbers $(n_\perp, n_\parallel)$ have been indicated. Planck constant values are in atomic units. The axes are the same as in Fig. 1.

which are perpendicular and parallel, respectively, to the minimum energy path. It can be assumed that these quantum numbers correspond to (ρ, ϑ) coordinates, so that $(n_\perp, n_\parallel) = (n_\rho, n_\vartheta)$. Thus, states $n = 9$ and $n = 17$ represented in Fig. 5 are examples of regular states excited in ϑ coordinate $(0, 12)$ and both ρ and ϑ coordinates $(1, 10)$, respectively. It is known [1] that these regular states $n = 1 - 23$ at $\hbar = 1$ a.u. corresponds to quantization on the undestroyed classical tori around $(\vartheta, P_\vartheta) = (\pi, 0)$ (rad, a.u.) elliptic point shown in Fig. 2.

Above state $n = 23$ at $\hbar = 1$ a.u., no more excitations in ϑ coordinate can be accommodated in the undestroyed classical tori around $(\pi, 0)$ (rad, a.u.) elliptic point, and states $n = 24$ and $n = 25$ represented in Fig. 5 are quantized, hence localized, on the unstable and stable 1:8 resonances, respectively, which are immersed in the chaotic sea, near to energy boundary, shown in the middle panel of Fig. 2. The corresponding periodic orbits (in red) have been superimposed over the wavefunctions, so that we can observe that wavefunctions are localized along the periodic orbits, and quantum numbers $(n_\perp, n_\parallel) = (0, 24)$ can be assigned by counting nodal lines which are perpendicular and parallel to the corresponding periodic orbit. Notice that a quantum eigenstate localized on an unstable periodic orbit is called a scarred state or just a scar.

Above states $n = 24$ and $n = 25$ at $\hbar = 1$ a.u., we go into the mixed-chaos region, where there exist regular states with additional excitations in ρ coordinate that can still be accommodated in the undestroyed tori around $(\pi, 0)$ (rad, a.u.) elliptic point shown in the right panel of Fig. 2, as is the case for the state $n = 32$ represented in Fig. 5. There also exist regular states quantized on classical tori around $(0, 0)$ elliptic point, as is the case for the state $n = 47$, and obviously there exist irregular or chaotic states related with the classical chaotic sea, which do not have a recognizable nodal pattern, so

that no quantum numbers can be assigned, as is the case for states $n = 38$ and $n = 60$.

Ultimately, observe that the scarred states $n = 24$ and $n = 25$ at $\hbar = 1$ a.u., which are in the vicinity of a *broad* avoided crossing (marked with an open circle in Fig. 4), recover the regular character at $\hbar = 0.8$ a.u., as is shown in Fig. 5.

Indeed, in the correlation diagram of the LiCN molecular system, as well as in that of the KCN system, the symmetry-derived non-crossing rule [10] is applicable, so that all crossings between eigenstates in Fig. 4 are avoided crossings, which involve Fermi resonances [11,12], although not all avoided crossings have the same behavior. Thus, in the left down region of the LiCN correlation diagram all crossings are *narrow* avoided crossings, and the involved eigenstates exchange their characters, so that mixing states (i.e., affected by the Fermi resonance) appear just at the immediate vicinity of the avoided crossing. Notice that, as energy and Planck constant increase in the LiCN correlation diagram, different series of Fermi resonances appear, being their order of resonance $\omega_\vartheta{:}\omega_\rho = |m_\rho - n_\rho|{:}|m_\vartheta - n_\vartheta|$ for involved states (m_ρ, m_ϑ) and (n_ρ, n_ϑ). The main ones of such series of resonances have been marked in the LiCN correlation diagram, and the corresponding order of resonance $\omega_\vartheta{:}\omega_\rho$ and quantum numbers (n_ρ, n_ϑ) of involved states have been detailed in Table 1. Observe the correspondence between the appearance of classical and quantum resonances as energy (and Planck constant) increases, namely 1:6, 2:14, 1:8, 2:18, 1:10, again 1:10, and 1:8.

However, the last 1:8 resonance series has a different behavior: As indicated above, it corresponds to a *broad* avoided crossing, and contrary to the other resonances the involved eigenstates do not exchange their characters, so that mixing states remain after the avoided crossing. This behavior leads to the energy-level repulsion, which is a feature of quantum chaos derived from random matrix theory [3]. Accrodingly, the 1:8 resonance series, where scarred states are originated, was stated as the (order-chaos) frontier of scars [13,14]. Behind the frontier of scars, i.e., in the right top region of the LiCN correlation diagram, level repulsion predominates, which corresponds to the classical chaotic sea. Nevertheless, in a similar fashion as classical tori emerge from the chaotic sea, regular eigenstates (characterized by narrow avoided crossings

Symbol	Resonance order $\omega_\vartheta{:}\omega_\rho$	Involved states (n_ρ, n_ϑ)
☆	1:6	$(0, 6+2k) \pm (1, 2k)$, $\{k = 0, 1, \ldots, 9\}$
△	2:14	$(0, 14+2k) \pm (2, 2k)$, $\{k = 0, 1, \ldots, 7\}$
◊	1:8	$(0, 8+2k) \pm (1, 2k)$, $\{k = 0, 1, \ldots, 9\}$
▽	2:18	$(0, 18+2k) \pm (2, 2k)$, $\{k = 1, 2, \ldots, 8\}$
□	1:10	$(0, 10+2k) \pm (1, 2k)$, $\{k = 2, 3, \ldots, 12\}$
◯	1:8	$(0, 8+2k) \pm (1, 2k)$, $\{k = 2, 3, \ldots, 12\}$

Table 1. Quantum numbers (n_ρ, n_ϑ) identifying the states involved in each series of Fermi resonances marked at the regular region of the correlation diagram of the LiCN molecular system represented in the left panel of Fig. 4.

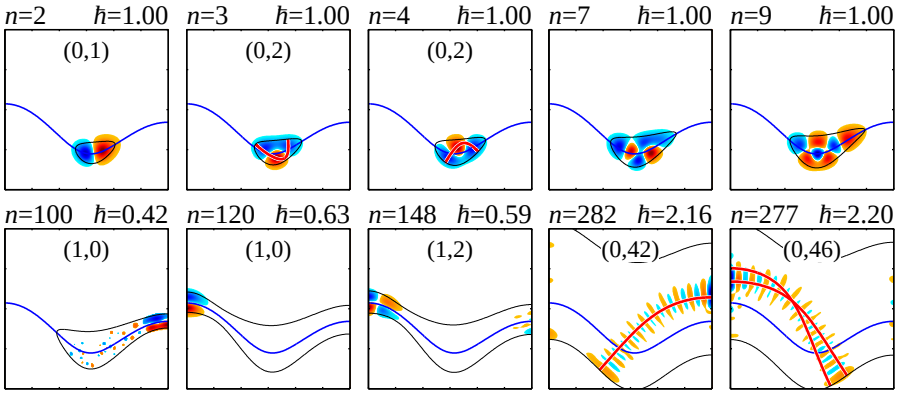

Fig. 6. Same as described in the caption of Fig. 5 for the KCN eigenstates.

with states characters exchange) emerge from the level repulsion sea. This is the case of the hyperbolic curves in the right top region of the LiCN correlation diagram, that correspond to regular states quantized on the classical tori around $(0,0)$ elliptic point, as is the case of the state $n = 47$ at $\hbar = 1$ a.u. mentioned above. However, in order to establish the correspondence between classical phase space structures and quantum correlation diagram in the mixed-chaos regime, we will turn to the KCN molecular system.

The correlation diagram of eigenenergies versus Planck constant for the KCN molecular system is depicted in the right panel of Fig. 4. Representative states at the true value $\hbar = 1$ a.u., as well as at other values for emerging regular states examples, have been marked with red dots and the corresponding wavefunctions depicted in Fig. 6.

Observe that, unlike the LiCN case, the correlation diagram for KCN system exhibits a widespread level repulsion feature, albeit some regular structures emerge from the level repulsion sea. Indeed, only ground state $n = 1$ (which is obviously Gaussian-like) and first excited state $n = 2$ (shown in Fig. 6 at $\hbar = 1$ a.u.) can be considered as regular states. This quantum behavior is related to the classical early destruction (at very low energy) of the main tori, as was shown in the first row of panels of Fig. 3.

Above state $n = 2$ at $\hbar = 1$ a.u., no more excitations in ρ and ϑ coordinates are supported, and similarly to states $n = 24$ and $n = 25$ of LiCN system discussed above, states $n = 3$ and $n = 4$ represented in Fig. 6 are quantized, hence localized, on the stable and unstable 1:2 resonances, respectively, which are immersed in the chaotic sea, as was shown in the second row of panels of Fig. 3. The corresponding periodic orbits (in red) have been superimposed over the wavefunctions, so that we can observe that wavefunctions are localized along the periodic orbits, and quantum numbers $(n_\perp, n_\parallel) = (0, 2)$ can be assigned by counting nodal lines which are perpendicular and parallel, respectively, to the corresponding periodic orbit. However, unlike states $n = 24$ and $n = 25$ of LiCN system, states $n = 3$ and $n = 4$ do not recover the regular character as $\hbar$ decreases to the numerically computable minimum value $\hbar = 0.1$

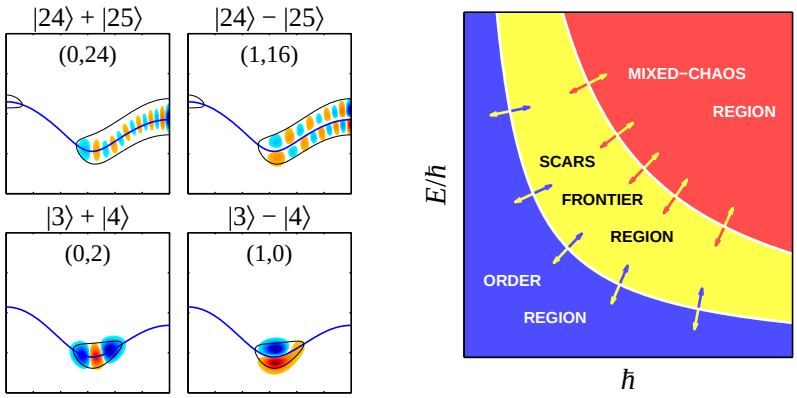

Fig. 7. (Left) Wavefunctions $\langle R\,\theta|n\rangle_{\hbar=1}$ of the sum and difference combination of the LiCN eigenstates $n = 24$ and $n = 25$ (upper panels) and the KCN eigenstates $n = 3$ and $n = 4$ (lower panels) unmixing states belonging to the scars frontier at $\hbar = 1$ a.u. (Right) Schematic correlation diagram ($E/\hbar$ versus $\hbar$) arrangement for a generic molecular system, showing the three possible different regions. Depending on the specific molecular system, the borderline between regions can move as indicated by the arrows.

a.u. In order to prove that states $n = 3$ and $n = 4$ are involved in a Fermi resonance, and then regular character is recovered for $\hbar < 0.1$ a.u., sum and difference combination of the involved states was calculated. As is shown in the left side of Fig. 7, in the same way as sum and difference combination of LiCN scarred states $n = 24$ and $n = 25$ at $\hbar = 1$ a.u. recover regular behavior with quantum numbers $(0, 24)$ and $(1, 16)$ [1:8 Fermi resonance], the combination of KCN scarred states $n = 3$ and $n = 4$ at $\hbar = 1$ a.u. recover regular behavior with quantum numbers $(0, 2)$ and $(1, 0)$ [1:2 Fermi resonance]. Notice that a more accurate unmixing can be performed by calculating the couplings $\langle m|\partial/\partial\hbar|n\rangle$, as was done in Ref. [13]. States $n = 5$ and $n = 6$, not represented in Fig. 6, have a similar behavior, albeit increasing excitation to quantum numbers $(n_\perp, n_\parallel) = (0, 3)$. So that, states from $n = 3$ to $n = 6$ at $\hbar = 1$ a.u. correspond to the frontier of scars in the KCN molecular system.

Above state $n = 6$ at $\hbar = 1$ a.u., most states correspond to irregular ones, as is the case of states $n = 7$ and $n = 9$ represented in Fig. 6. However, as was indicated above, regular quantum structures corresponding to classical tori emerge from the chaotic level repulsion sea. Thus, as energy and Planck constant increase, two sets of hyperbolic curves constituted by narrow and very narrow, respectively, avoided crossings emerge. The first of them, in which hyperbolic curves are slightly diffuse due to the avoided crossings are broader, corresponds to regular states quantized on the tori that, surprisingly, appear at the linear saddle configuration ($\vartheta = \pi$ rad), as was shown in the third row of panels of Fig. 3. State $n = 100$ at $\hbar = 0.42$ a.u. with quantum numbers $(1, 0)$ represented in Fig. 6 is a representative of these regular states. Notice that, for this set, only excitations in ρ coordinate are allowed. Moreover, the second set of hyperbolic curves corresponds to regular states quantized on

the tori that appear at the linear minimum configuration ($\vartheta = 0$), as is the case for states $n = 120$ at $\hbar = 0.63$ a.u. with quantum numbers $(1, 0)$, and $n = 148$ at $\hbar = 0.59$ a.u. with quantum numbers $(1, 2)$, both represented in Fig. 6. Notice that, for this set, the first excitation in ϑ coordinate is allowed. On the other hand, also two sets of mostly straight lines, formed by narrow avoided crossings, with clearly different slopes, emerge from the chaotic level repulsion sea in the right top region of the KCN correlation diagram. These sets correspond to states localized on the *hinge* motion tori that were shown in fourth row of panels of Fig. 3. States $n = 282$ at $\hbar = 2.16$ a.u. with quantum numbers $(0, 42)$, and $n = 277$ at $\hbar = 2.20$ a.u. with quantum numbers $(0, 46)$ in Fig. 6, are representatives of each hinge motion type. Observe that, in fact, both wavefunctions are localized along the corresponding periodic orbits shown in Fig. 6.

Finally, we could establish a schematic correlation diagram arrangement for a generic molecular system as that depicted in the right side of Fig. 7, where the quantum transition from order to chaos is represented. Observe that in Fig. 4, the three regions (order, scars frontier, and mixed-chaos) are clearly represented in the LiCN correlation diagram. However, in the KCN correlation diagram, mainly the chaotic (mixed-chaos) region is shown, being the order region and the frontier of scars mainly shrunk into not calculated range $0 < \hbar < 0.1$ a.u.

4 Concluding remarks

We have established the quantum-classical correspondence for nonlinear molecular systems, by analyzing the structures of the classical phase space and the quantum correlation diagram of eigenenergies versus Planck constant.

The relationships found are in order. Each Poincaré-Birkhoff resonance in the regular region of phase space corresponds to a series of Fermi resonances in correlation diagram. The highest classical action resonances, immersed in the chaotic sea, correspond to the quantum resonances that constitute the frontier of scars. The chaotic sea in phase space corresponds to the level repulsion region (overlap of broad avoided crossings) in correlation diagram, where the regular tori that emerge from the chaotic sea (mixed-chaos) correspond to states formed by narrow avoided crossings that emerge from the level repulsion sea.

References

1. J. B. Keller. Semiclassical mechanics, *SIAM Review*, **27**, 485, 1985.
2. M. C. Gutzwiller. Classical quantization of a Hamiltonian with ergodic behavior, *Physical Review Letters*, **45**, 150, 1980.
3. M. L. Mehta. *Random Matrices*, Elsevier, Amsterdam, 2004.
4. F. J. Arranz, F. Borondo, and R. M. Benito. Scar formation at the edge of the chaotic region, *Physical Review Letters* **80**, 944, 1998.
5. R. Essers, J. Tennyson, and P. E. S. Wormer. An SCF potential energy surface for lithium cyanide, *Chemical Physics Letters*, **89**, 223, 1982.
6. H. Párraga, F. J. Arranz, R. M. Benito, and F. Borondo. *Ab initio* potential energy surface for the highly nonlinear dynamics of the KCN molecule, *Journal of Chemical Physics*, **139**, 194304, 2013.

7. F. J. Arranz, R. M. Benito, and F. Borondo. The onset of chaos in the vibrational dynamics of LiNC/LiCN, *Journal of Chemical Physics*, **123**, 134305, 2005.
8. Z. Bačić and J. C. Light. Highly excited vibrational levels of "floppy" triatomic molecules: A discrete variable representation–Distributed Gaussian basis approach, *Journal of Chemical Physics*, **85**, 4594, 1986.
9. A. J. Lichtenberg and M. A. Lieberman. *Regular and Chaotic Dynamics*, Springer, New York, 1992.
10. T. Inui, Y. Tanabe, and Y. Onodera. *Group Theory and Its Applications in Physics*, Springer, Berlin, 1990.
11. E. Fermi. Über den ramaneffekt des kohlendioxyds, *Zeitschrift für Physik*, **71**, 250, 1931.
12. G. Herzberg. *Molecular Spectra and Molecular Structure. Vol II: Infrared and Raman Spectra of Polyatomic Molecules*, Van Nostrand, New York, 1959.
13. F. J. Arranz, F. Borondo, and R. M. Benito. Avoided crossings, scars, and transition to chaos, *Journal of Chemical Physics*, **107**, 2395, 1997.
14. F. J. Arranz, L. Seidel, C. G. Giralda, R. M. Benito, and F. Borondo. Scars at the edge of the transition from order to chaos in the isomerizing molecular systems LiNC-LiCN and HCN-HNC, and HO_2, *Physical Review E*, **82**, 026201, 2010.